Case Studies in Construction Materials 18 (2023) e01789

Contents lists available at ScienceDirect

Case Studies in Construction Materials

journal homepage: www.elsevier.com/locate/cscm

Case study

Numerical and theoretical research on flexural behaviour of steel-precast UHPC composite beams

Wenjie Ge [a,b], Chi Liu [a], Zhiwen Zhang [a,*], Zhongwei Guan [c], Ashraf Ashour [d], Shoutan Song [e], Hongbo Jiang [a], Chuanzhi Sun [b], Linfeng Qiu [f], Shan Yao [g], Weihua Yan [a], Dafu Cao [a]

[a] College of Civil Science and Engineering, Yangzhou University, Yangzhou 225127, China
[b] Jiangsu Province Engineering Research Center of Prefabricated Building and Intelligent Construction, Suqian 223800, China
[c] School of Engineering, University of Liverpool, Liverpool L693GQ, UK
[d] School of Engineering, University of Bradford, Bradford BD71DP, UK
[e] College of Civil Engineering, Southeast University, Nanjing 225009, China
[f] Nantong Construction Quality and Supervision Station, Nantong 226000, China
[g] Gansu Engineering Design and Research Institute Co., LTD., Lanzhou 730030, China

ARTICLE INFO

Keywords:
Flexural performance
Composite beam
Ultra-high performance concrete
Section steel
Bearing capacity

ABSTRACT

In order to promote the utilization of high strength materials and application of prefabricated structures, flexural behaviour of section steel-precast UHPC (Ultra-High performance concrete) slab composite beams prefabricated with bolt shear connectors are numerically simulated by the finite element (FE) software ABAQUS. The model is verified by three prefabricated steel-concrete composite beams tested. Numerical analysis results are in good accordance with experimental results. Furthermore, parametric studies are conducted to investigate the effects of strength of section steel and concrete of precast slab, thickness of section steel, width and height of precast concrete slab, diameters of steel bars and bolt shear connectors. The flexural behaviour of composite beams, in terms of bearing capacity, deflection, ductility and energy dissipation, are compared. The numerical results indicate that the improvement of strength of section steel results in a decrease of ductility, but a significant increase of the ultimate load and energy dissipation. Compared with composite beam made of section steel with thickness of 10 mm, the ultimate load of beams made of section steel with thickness of 14 and 18 mm improve by 29.0% and 58.8%, respectively, the ductility enhance by 2.8% and 8.3%, respectively, and the energy dissipation improve by 8.0% and 12.3%, respectively. With the increase of concrete strength, the ultimate load, deflection and energy dissipation gradually increase. The ductility of steel-UHPC composite beam is the highest, that of steel-HSC composite beam is the lowest. The effect of reinforcement ratio of concrete slab and diameter of shear bolts on the ultimate load of composite beam is limited. Simplified formulae for two different sectional types of proper-reinforced section steel-precast UHPC slab composite beams occurred bending failure are proposed, and the predicted results fit well with the simulated results. The results can be taken as a reference for the design and construction of section steel-precast UHPC slab composite beams.

* Corresponding author.
E-mail address: dx120220103@stu.yzu.edu.cn (Z. Zhang).

https://doi.org/10.1016/j.cscm.2022.e01789
Received 15 October 2022; Received in revised form 13 December 2022; Accepted 17 December 2022
Available online 19 December 2022

1. Introduction

Steel-concrete composite beam which combined steel beam with concrete slab, can sustain loads and deform coordinately as a whole structure. The steel beam is usually set in the tension area while concrete slab is located in compression zone, and the two are connected as a whole force-resistant system with shear connectors on-top of the steel beam. Steel-concrete composite beam has the advantages of good mechanical performance, saving steel consumption, energy conservation and environmental protection, reducing construction cost, achieving a large span space and so on. With the increase of the building of high-rise buildings and long span structures, the Steel-concrete composite beams have been widely used.

Steel-concrete composite beams fully utilizes the compression of concrete and tension of steel, have the following advantages. 1) Technology advantage: compared with normal reinforced concrete (RC) beam, the composite beam has low height and light weight. Compared with section steel beam, the composite beam has small cross-section of steel a layer of added concrete slab, leads to an enhancement of lateral and vertical stiffness and a reduction of deformation under live load as well as an improvement of fire resistance, durability, stability and integrity. 2) Good economic benefits: the composite beam can save materials effectively. According to engineering experience, the steel consumption of composite beam reduces by 15～20% compared with that of section steel beam, and the cost decreases by 10～40%. When compared with RC beam, the height of structure reduces by 1/3–1/4, the self-weight decreases by 40～60%. In addition, the steel beam acts as a template in the construction stage, results in a reduction of consumption of templates and construction cost. 3) Good social benefits: compared with RC beam, the composite beam bridge has the advantages of low self-weight and large span, reduces the impact on the traffic under the bridge. And some components of the composite beams can be reused, meets the conception of low carbon construction and sustainable development. The composite beam bridge also has low driving noise when compared with steel beam bridge. 4) Short construction period and fast construction speed: using the steel beam as temporary template allows concrete templates to be directly placed on it, thereby accelerating construction. The steel beam and concrete slab can be prefabricated in the factory and assembled on-site, the amount of cast-in-place is reduced.

Although the steel-concrete composite beam has many advantageous when compared with RC beam and steel beam, its shortcomings causes by the limits of materials cannot be ignored. The concrete slab easy to crack under tension decreases its durability. The mechanical performance of concrete degrades under corrosion service environments, decreases the bearing capacity and structural safety, increases the maintenance cost in service stage. After a long-term service, the concrete slab usually cracks near the shear connectors for the composite beam under the fatigue effect of repeated load and impact effect of dynamic load. The shear connectors are easy to corroded and the durability of composite beam decreases. Excessive slip (between the steel beam and concrete slab) can't effectively ensure the deformation compatibility of the combined system composed of steel beam and concrete slab, weakens the overall working performance of composite beams. It can be found that the shortcomings of steel-concrete composite beam mainly result from the defects of ordinary concrete. In order to overcome the shortcomings, Ultra-High Performance Concrete (UHPC) [1] with excellent mechanical properties (high compressive and tensile performances), high toughness and good durability is used to replace normal concrete, to from section steel-UHPC composite beam. Wang et al. [2] explored the mechanical performance of bolted shear connections embedded in concrete composite beams by conducting the push-off tests. Studies shows with the increase of the bolt pretension, the initial slip load and the shear stiffness per bolt connector significantly improved, but the bolt shear capacity slightly changed. The shear strength and peak slip as well as shear stiffness per bolt connection improved with the increase of the bolt diameter. Test results carried out by Ma et al. [3] showed the stud connectors had good shearing resistance, deformation performance and ductility. Bolted connectors also had features of construction and installation-friendly, ensuring effective connection and improving construction efficiency. Zhang et al. [4] numerical study to investigate the flexural performance of simply-supported layered ultra-high performance concrete-normal strength concrete (NSC) beams consisting of two UHPC layers with an NSC core layer sandwiched in between. The numerical results show that with properly designed UHPC layer thickness, the beam with a thick NC core layer can not only sustain the same loading as a pure UHPC beam with the same thickness but is also much less costly. Yu et al. [5] investigated the artificial intelligence (AI) models to analysis the shear transfer mechanism of steel fiber reinforced concrete (SFRC) beams without stirrups. The results indicate that the shear capacity depends heavily on the material properties of concrete, the amount of longitudinal reinforcement, the attributes of steel fibers, and the geometrical and loading characteristics of SFRC beams.

The results obtained by Pathirana et al. [6] indicated that the ability of blind bolts to achieve and maintain composite action in steel-concrete beams was comparable to that of welded stud connectors. The report studied by Yan et al. [7] exhibited that the flexural behaviour of U-shaped steel-encased concrete composite beam (SUSCCB) was superior to that of a traditional U-shaped steel-encased concrete composite beams (USCCB). Yang et al. [8] found that shear connector welds were not necessary in the web-embedded steel-concrete composite beam (WTSCB) when compared with ordinary composite beam, and WTSCBs occurred bending failure exhibited excellent deformability. Gao et al. [9] studies indicated the shallow composite beams had a high flexural capacity and ductility, and the beam with partial shear connections had a good ability of stress redistribution. Lou et al. [10] comprehensively evaluated the inelastic behavior of continuous steel-concrete composite (SCC) beams. The results showed that the crack width in concrete slab of beam with carbon fiber reinforced polymer (CFRP) reinforcement was less than those of beams with steel or glass fiber reinforced polymer (GFRP) reinforcement. The ultimate load of beams with CFRP reinforcement was close to that of specimen with steel reinforcement, but greater than that of specimen with GFRP reinforcement. Compared with beams with steel reinforcement, GFRP reinforcement led to comparable moment redistribution but lower moment, CFRP reinforcement resulted in substantially lower moment redistribution but greater support moment. Experimental results conducted by Idris et al. [11] illustrated that DSTB (double-skin tubular beam, that is fiber reinforced polymer (FRP)-high-strength concrete (HSC)-steel composite beam) was capable of developing a great inelastic deformation. The diameter and thickness of the inner steel tube had a significant effect on flexural behaviour of DSTBs. Increasing the concrete strength and concrete-filling the inner steel tube enhanced the bearing capacity of DSTB

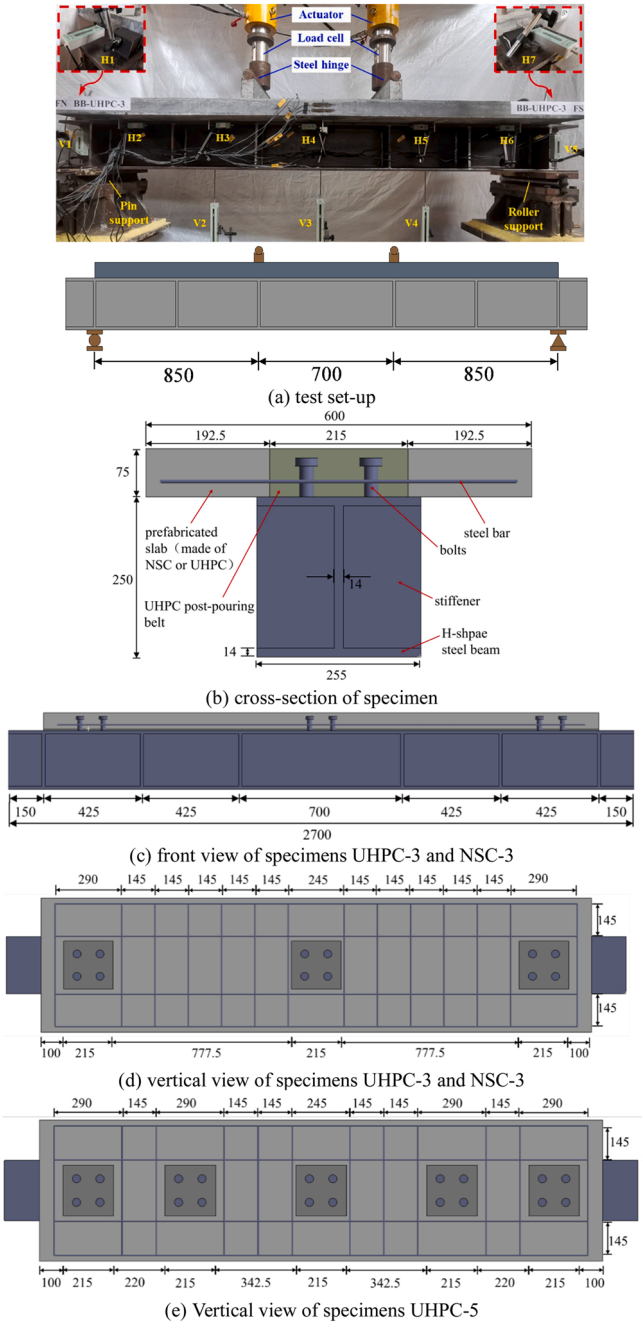

Fig. 1. Diagrammatic sketch of models established.

without affecting their overall ductility. Xiong et al. [12] claimed that the high-strength steel-precast concrete slab (HSS-PCS) composite beams with steel block shear connectors (SBSCs) had good integral working capacity with high bearing capacity and stiffness.

Experimental results reported by Fan et al. [13] illustrated crack resistance and flexural stiffness for the steel-ECC (Engineered Cementitious Composites) composite beams were significant improved. Test results of Nguyen et al. [14] indicated that when comparing with the NSC (normal strength concrete)-HSS beam, the bearing capacity of ECC-HSS (high strength steel) composite beam increased slightly, but the ductility obviously improved. The NSC-HSS composite beam failed in a less ductile manner with a sudden crushing of NSC and a sharp drop of bending resistance after the peak load. All ECC-HSS composite beams failed in a ductile mode and exhibited gradual softening after the peak load. Hu et al. [15] held that the steel and UHPC had good composite action, and the flexural behaviour of steel-UHPC composite beams were obviously enhanced. Zhang et al. [16] claimed that steel-UHPC composite beams illustrated good cracking and flexural behaviour under the hogging moment. Compared with the steel-NSC composite beam, cracking

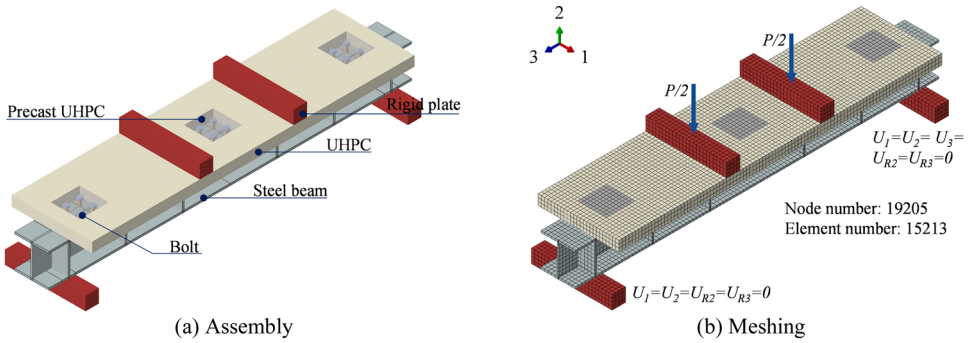

Fig. 2. Three-dimensional FE model.

and ultimate loads of steel-UHPC composite beams increased by 340% and 26%, respectively. Zhu et al. [17] found that comparing with reducing the number of ribs, the decreasing of thickness of upper panel for waffle slab significantly increased the risk of longitudinal splitting failure and weakened its integrity. The waffle slab with low ribs was recommend to used as the bridge deck. The increase of transverse reinforcement ratio had slight effect on improving the bearing capacity, but significantly on enhancing the deformation capacity. Liu et al. [18] reported that compared with S (steel)-RC (reinforced concrete) specimen, S (steel)-RC (reinforced concrete)-UHPC (ultra-high-performance concrete) specimen had a high bearing capacity and flexural stiffness. Moreover, specimen S-RC-UHPC had a low material cost and self-weight when compared with specimen S-RC. This validates the application prospect of S-RC-UHPC girders instead of S-RC or S-UHPC girders. Experimental results conducted by Fang et al. [19] showed that the cracking and failure patterns of the steel-UHPC composite beams were mainly dependent on the degrees of shear connection and the types of slab concrete. The composite beams with UHPC slabs exhibited higher cracking resistance, bearing capacity and ductility than those with normal-strength concrete slabs. Experimental results carried out by Tong et al. [20] showed that the failure mode of composite beam with full shear connections was the crushing of UHPC slab at the loading point. For steel-UHPC composite beam with partial shear connections, the failure mode was stud rupture. Zhang et al. [21] investigated the shear behaviors of high-strength friction-grip bolts (HSFGBs) under combined shear and tensile forces in steel-steel fiber reinforced concrete (SFRC) composite beams. The experimental results show that the both shear deformation and necking phenomenon of HSFGBs occurred under combined shear and tensile forces. The group-stud arrangement was applicable for the assembly construction. Studies performed by Shao et al. [22] showed that compared with steel-concrete beams, the hot rolled shape steel-ultrahigh performance concrete composite beam had lighter weight, lower cost and better constructability. Wang et al. [23] proposed a new kind of continuous composite beam composed of steel box-girder and UHPC waffle slab. The UHPC waffle slab increased the bearing capacity and span of structure, and reduced the risk of cracking.

Current studies are focus on the mechanical performance of steel-normal concrete composite beams, investigation on the mechanical performance of section steel-precast UHPC composite beams is limited. Fang et al. [19] experimental studied the flexural performance of three prefabricated steel-UHPC composite beams. The parameters of the test included the types of precast concrete and pocket concrete, as well as the numbers of shear connectors. The testing of influence factors considered was limited, important factors, including the mechanical properties of concrete and section steel, size of precast concrete slab and section steel, diameter of bolt shear connectors, were not considered. As a consequence, it is necessary to conduct a comprehensive study on the flexural behavior of composite beams with different sizes and strengths of concrete (UHPC and NSC) and section steel.

In this paper, three prefabricated steel-UHPC composite beams tested by Fang et al. [19] were numerically verified. The composite beam is composed of precast concrete slab and steel beam with shear bolts, and these two parts were assembled by cast-in-place UHPC. The concrete plastic damage model was used to simulate the damage behavior of concrete. Additionally, 21 models were established to analyze the effect of mechanical performance section steel and concrete, thickness of section steel, diameters of steel bars and shear bolts, width and height of concrete slab, on the bearing capacity, deflection, ductility and energy dissipation of composite beams based on the verified model. Furthermore, based on reasonable assumptions and simplified constitution models of materials, three failure modes and two boundary failure states of section steel-UHPC composite beams are proposed. And simplified formulae for two different types of section proper-reinforced composite beams occurred bending failure are put forward; the predicted results are in good accordance with simulated results. It is expected that this study will promote technological support for the application of steel-UHPC composite beams in engineering structures and serve as a reference for the structural design and construction of composite beams.

2. Establishment of 3D FE model

Three prefabricated section steel-concrete/UHPC composite beams [19] conducted are used to verify the model established. The detailed information is show in Fig. 1. The materials of precast concrete slab (the gray part in Fig. 1b) of NSC-3, UHPC-3 and UHPC-5 are NSC (normal strength concrete), UHPC and UHPC, respectively. The post-pouring belts (that is the cast-in-place parts shown green in Fig. 1b) of the composite beams were all poured with UHPC, and their numbers are 3, 3 and 5, respectively. The height, width and length of section steel beam (the blue part in Fig. 1c) are 250, 255 and 2700 mm, respectively. The length of free span and clear span

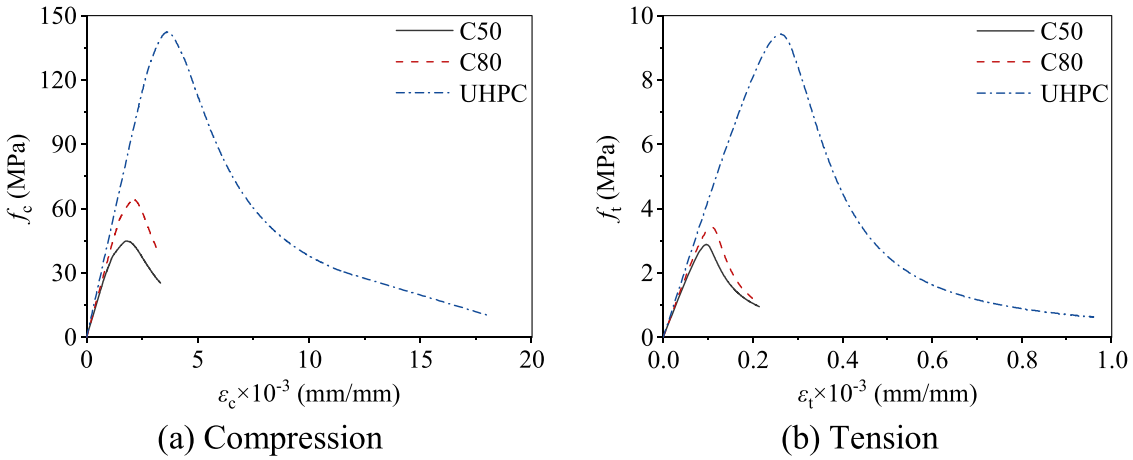

Fig. 3. Stress-strain curves of NSC and UHPC.

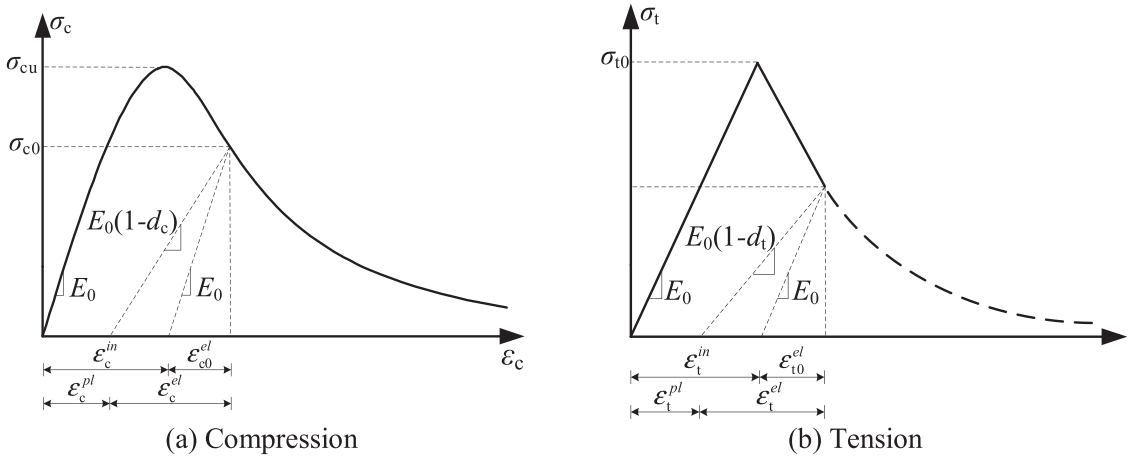

Fig. 4. Concrete damage plasticity constitutive (CDP) model.

are 150 and 2400 mm, respectively, and the length of bending-shear span and pure bending are 850 and 700 mm, respectively. The thickness of flange, web and stiffener of steel beam are all 14 mm. The bolt (grade M15) with diameter of 22 mm and length of 60 mm was adopted as shear connector. The diameter of the steel bar embedded in the precast concrete slab is 6 mm. The manufacturing process of composite beam is clarified as follows, 1) the bolts were welded onto the section steel beam; 2) the precast slab was poured with NSC/UHPC and cured, then the concrete template was removed when the concrete reached the acquired strength; 3) the precast slab was assembled onto the section steel beam, and the parts welded with bolts were poured with UHPC.

2.1. Interaction and boundary conditions

Fig. 2 illustrates the three-dimensional FE model (specimen UHPC-3 for example). The finite element (FE) software ABAQUS was utilized to investigate the flexural behavior of prefabricated section steel-UHPC composite beams. The standard solver (static, general) is adopted. In order to accurately simulate the contact settings between the components, the model was built in separate mode. The displacement-controlled loading method is used. To achieve an accurate calculation, the displacement increment control method is adopted during the analysis process.

The interaction between the constituent parts of the numerical model is performed using interaction and constraint options available in ABAQUS. In the model, the rebar skeleton and concrete are well bonded [19], so the slip between the reinforcement skeleton and concrete is disregarded, and the "Embedded Region" is used. Rigid constraint is used between the steel plate and the reference point. In the region of contact between the concrete slab and the top flanges of the steel beam, tangential contact of the "Hard contact-Penalty" type is considered, which employs the classic Lagrange multiplier method [24] to impose restrictions, and normal contact with friction coefficient equal to 0.6 [6] between steel beam and concrete is included. For interaction between the lower point of the headed shear bolt and the top flange of the steel beam, the “Tie constrain” tool is used, which simulates the welded connection between these two elements.

Table 1
Concrete damage plasticity parameters of NSC and UHPC.

Types of concrete	Ψ	ϵ	σ_{b0}/σ_{c0}	K_c	μ
NSC	38°	0.1	1.167	1/3	0.0005
UHPC	56°	0.1	1.16	1/3	0.0005

Note: Ψ is the dilation angle in degrees; ϵ is the flow potential eccentricity; μ is the viscosity parameter that defines viscoelastic regularization; K_c is the ratio of the second stress invariant on the tensile meridian to that on the compressive meridian; σ_{b0}/σ_{c0} is the ratio of the initial equiaxial compressive yield stress to the initial stress.

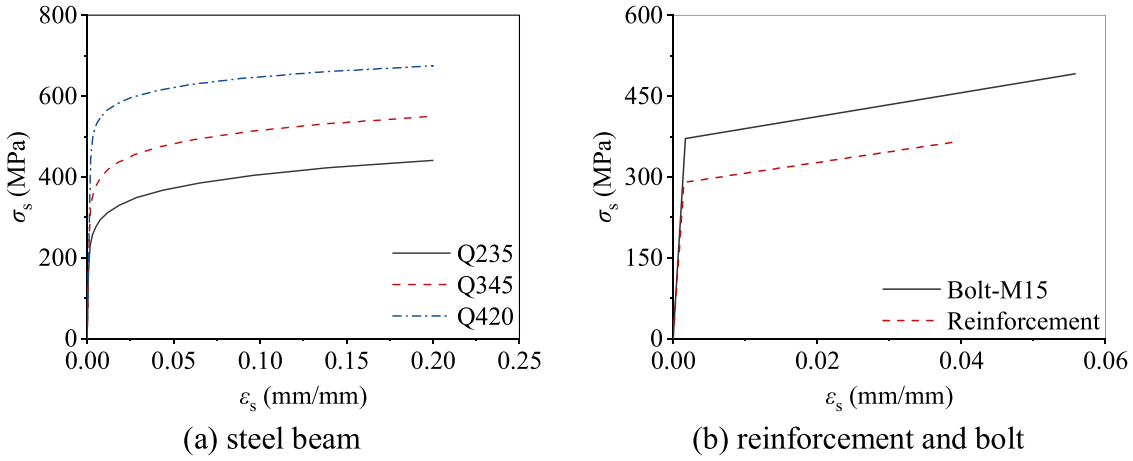

Fig. 5. Stress-strain curves of steel beam, reinforcement and bolt.

2.2. Material properties

2.2.1. NSC & UHPC

Fig. 3 shows the stress-strain curves of NSC and UHPC. The compressive and tensile stress-strain curves of NSC and UHPC are referred to "Code for design of concrete structures" (GB 50010–2010) [25] and Shan et al. [26], respectively. The peak compressive strains of C50, C80 [25] and UHPC [26] are 0.0020, 0.0022 and 0.0036, respectively, while their ultimate strains are 0.0032, 0.003 and 0.005, respectively.

The concrete damage plasticity constitutive (CDP) model [27,28], as shown in Fig. 4, is used and the specific parameters are shown in Table 1. Equation (1) expresses the damage variables for tension (d_t) and compression (d_c). These two parameters vary from 0 to 1, which use to characterize the degradation of the stiffness of the material, for undamaged state, the value equals to 0, and that is 1.0 for fully damaged state. ε_{pl}^{c} and ε_{pl}^{t} are the equivalent plastic strains in compression and tension, respectively. E_0 is the initial (undamaged) modulus of elasticity.

$$\begin{cases} \sigma_c = (1-d_c)E_0\left(\varepsilon_c - \varepsilon_c^{pl}\right) \\ \sigma_t = (1-d_t)E_0\left(\varepsilon_t - \varepsilon_t^{pl}\right) \end{cases} \tag{1}$$

2.2.2. Steel beam, bolt and steel bar

Fig. 5 shows the stress-strain curves of steel beam, reinforcement and bolt. It can be observed from the experimental phenomenon [19] that the steel beam did not deform greatly during the bending process, and the lower flange didn't rupture due to tensile stress. Therefore, the softening behavior of Q235 steel is ignored. The Ramberg-Osgood model [29] is used for steel beam, while the ideal elastic-plastic model of reinforcement and bolt is adopted.

2.3. Sensitivity analysis of grid size

The three-dimensional eight-node solid element (C3D8R), which has three translational degrees of freedom at each node, is used for the concrete. The two-node three-dimensional truss element (T3D2) is used for reinforcement and bolt. The shear deformation in the transverse direction (thickness) has limited effect on a thin shell when its thickness to length ratio is less than 1/15. The four-node normal shell element (S4R) is used for the steel beam. Taking specimen UHPC-3 for example, the concrete is meshed by 15, 25, 35 and 50 mm, respectively, and the steel beam, steel skeleton and bolts are meshed by 25, 2 and 2 mm, respectively. The analysis of the mesh sensitivity is exhibited in Fig. 6 based on the load-displacement curves of specimens UHPC-3 with different element sizes, where the suffix "E" and "S" represent experimental and simulated results, respectively.

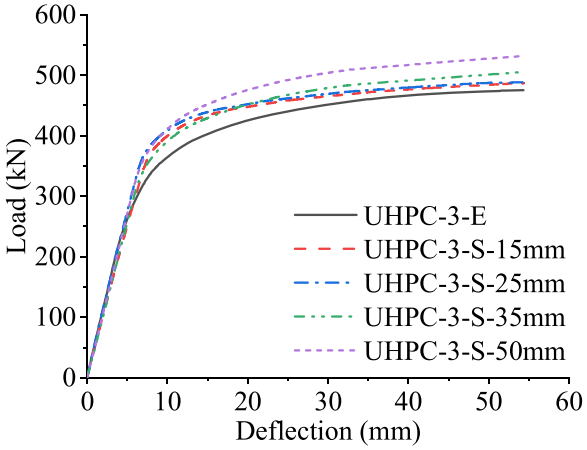

Fig. 6. Load-deflection curves of specimen UHPC-3 with various element sizes.

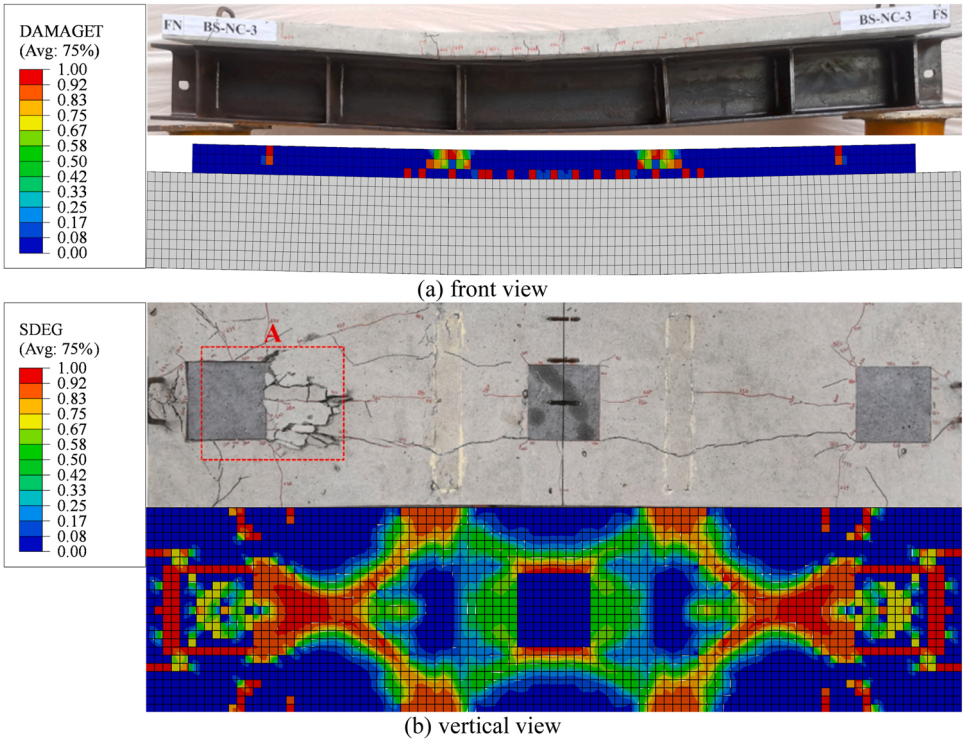

Fig. 7. Comparison of the experimental and simulated failure pattern of specimen NSC-3.

Compared with the test results, the calculated results of models with 35 mm and 50 mm grids are larger, whereas those of model with 15 mm and 25 mm grid are similar. In order to ensure the accuracy of the simulate results and reduce the computational cost simultaneously, grid with 25 mm is used to model the concrete.

3. Model verification

3.1. Experimental phenomena and failure pattern

The comparisons of the experimental and simulated failure patterns of specimens NSC-3, UHPC-3 and UHPC-5 are shown in Figs. 7, 8 and 9, respectively.

For specimen NSC-3, the cracks first occur at the sides (longitudinal direction) of post-pouring belts. With the increase of load applied, the cracks gradually developed to both sides. Finally, the concrete on top of the precast slab nears the post-pouring belt is

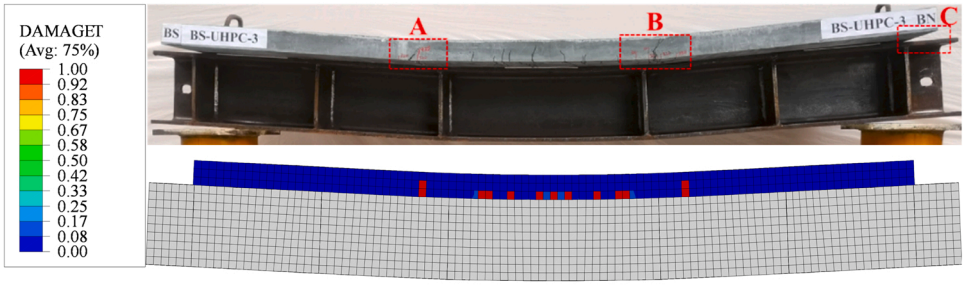

(a) front view

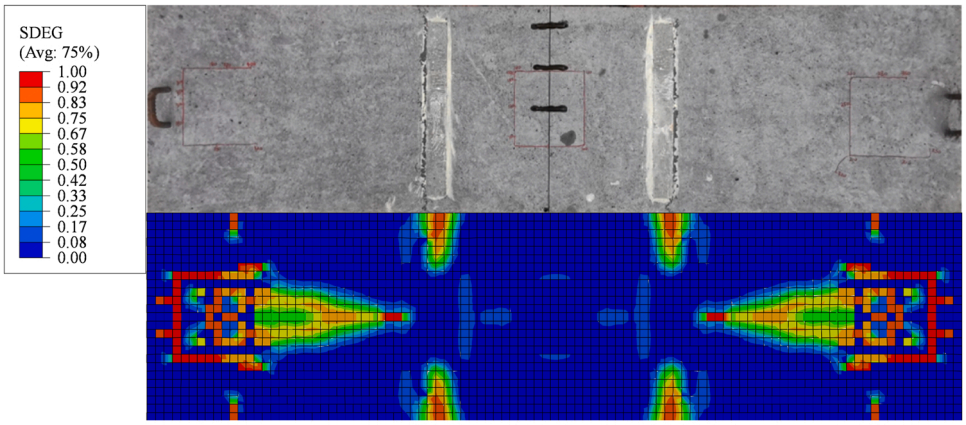

(b) vertical view

Fig. 8. Comparison of the experimental and simulated failure pattern of specimen UHPC-3.

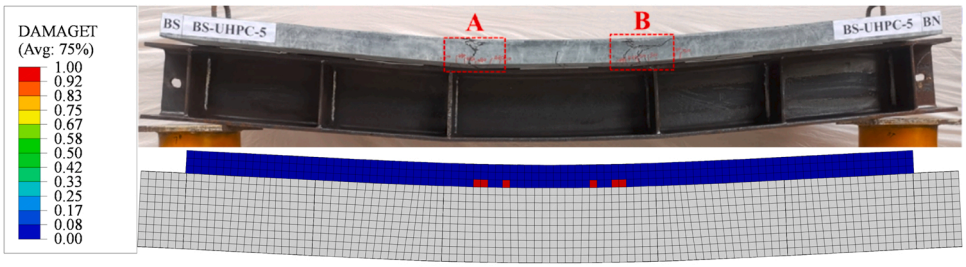

(a) front view

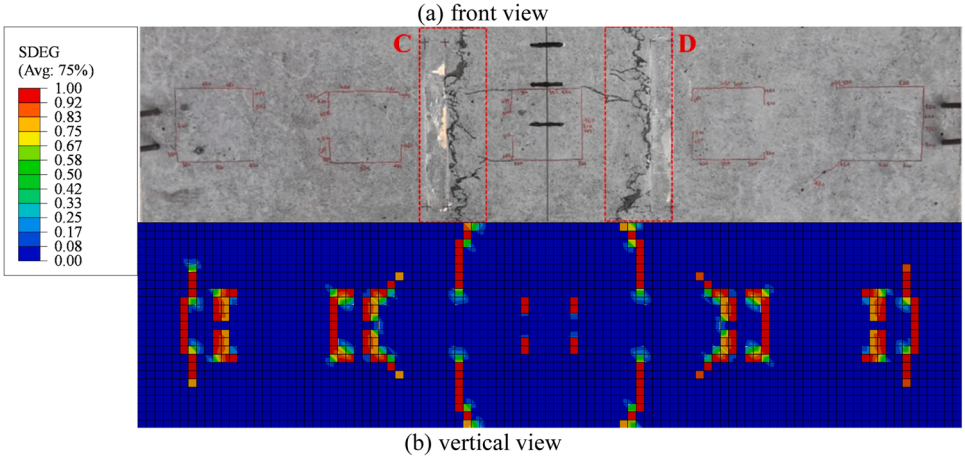

(b) vertical view

Fig. 9. Comparison of the experimental and simulated failure pattern of specimen UHPC-5.

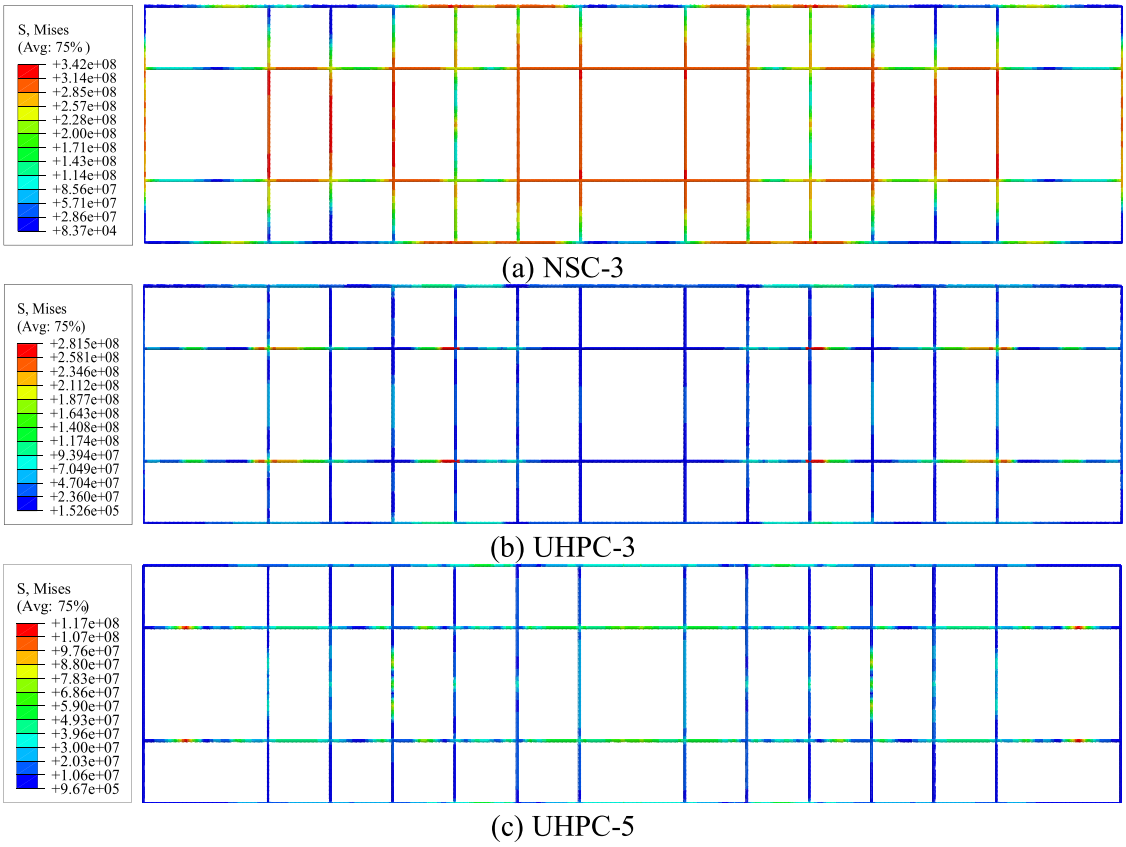

Fig. 10. Von Mises stress contour of steel bars.

crushed, the post-poured UHPC not occur obvious damage. For specimen UHPC-3 and UHPC-5, the cracks also first occur at the sides of post-pouring belts. With the increase of load applied, the widths of cracks increase gradually, slightly develop to both sides. Finally, with the increase of load applied, the shear bolts at both sides fail and composite beam reach its shear bearing capacity.

The Von Mises stress contour of steel bars embedded in the concrete slab is shown in Fig. 10.

The observation from Fig. 10a show that for specimen NSC-3, the maximum plastic strains locate at sides of post-pouring belts where the cracks occur. The concrete slab and steel bar embedded sustain the compression together first. The steel bar bore more compression when top concrete crushed and out of work. For specimen UHPC-3 (Fig. 10b), the precast concrete slab made of UHPC can sustains larger compression when compared with that made of NSC. The steel bars at the side of post-pouring belts occur obvious deformation, and the strains of steel bars at the mid-span reach ultimate compressive strain. For specimen UHPC-5 (Fig. 10c), the number of post-pouring belts is greater than that of specimen UHPC-3, the bearing capacity is significantly improved. The strains of mid-span steel bars reach ultimate compressive strain.

The equivalent plastic strain distribution of section steel is shown in Fig. 11.

As observed from the figure that the tensile yield starts from both sides of the lower flange of section steel, and gradually extends to the mid-span, and extends upward. The deformation of NSC-3 is the smallest, that of UHPC-3 is larger, and that of UHPC-5 is the largest. The lower flanges of the section steel in three beams all reach ultimate tensile strain at the time of failure.

The Von Mises stress contour of the bolts is shown in Fig. 12.

It can be seen from the figure that the stress at the mid-span of UHPC-3 is lower than that of NSC-3. The compressive performance of UHPC slab is better than that of NSC slab, UHPC-3 has a larger bearing capacity than specimen NSC-3 accordingly, the bolts in specimen UHPC-3 sustain greater shear stress. As the number of bolts of specimen UHPC-5 is greater than that of specimen UHPC-3, the maximum shear force of each bolt in UHPC-5 is lower than that in UHPC-3, the bearing capacity of specimen UHPC-5 is improved correspondingly.

3.2. Load-deflection curve and ductility

The comparison between the simulated and experimental load-deflection curves is shown in Fig. 13. The comparisons between the experimental and simulated yield and ultimate loads, corresponding deflections and ductility are shown in Table 2, where P_y (here, equal energy method is adopted to determine equivalent yield point [30]) and P_u are the yield and ultimate load, respectively, d_y and

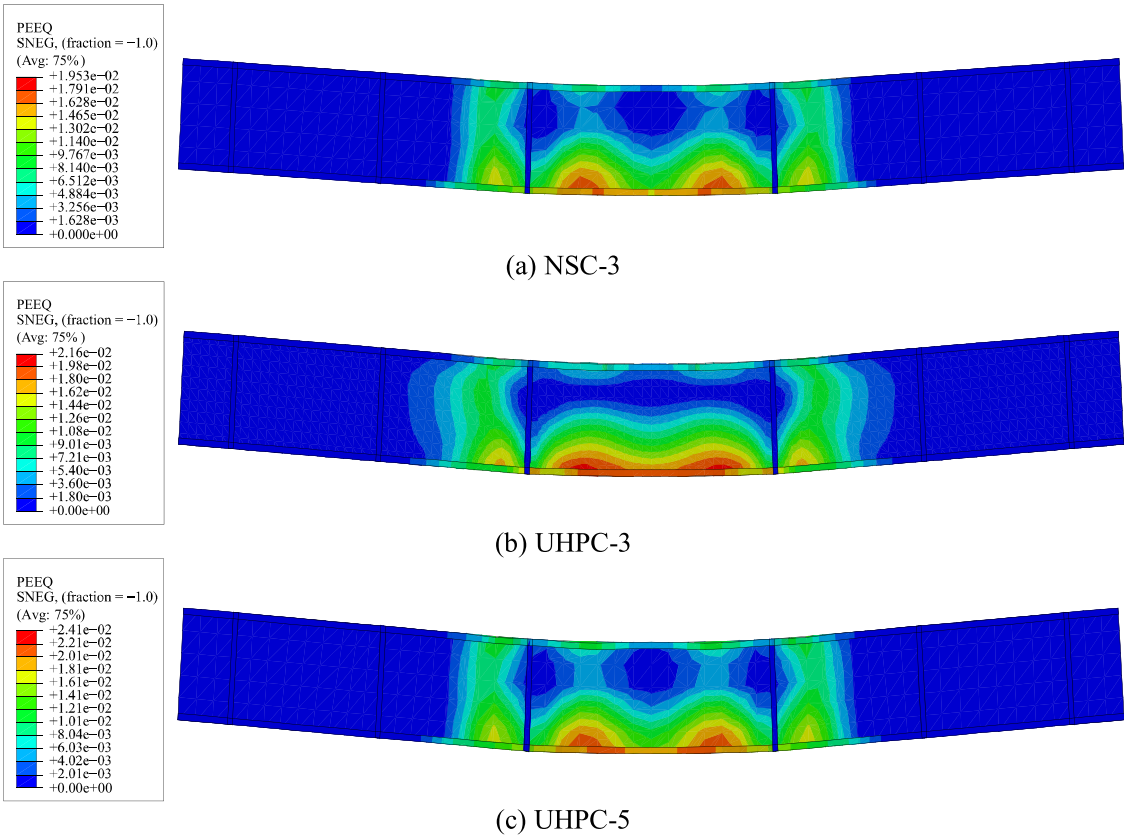

Fig. 11. Equivalent plastic strain distributions of section steels.

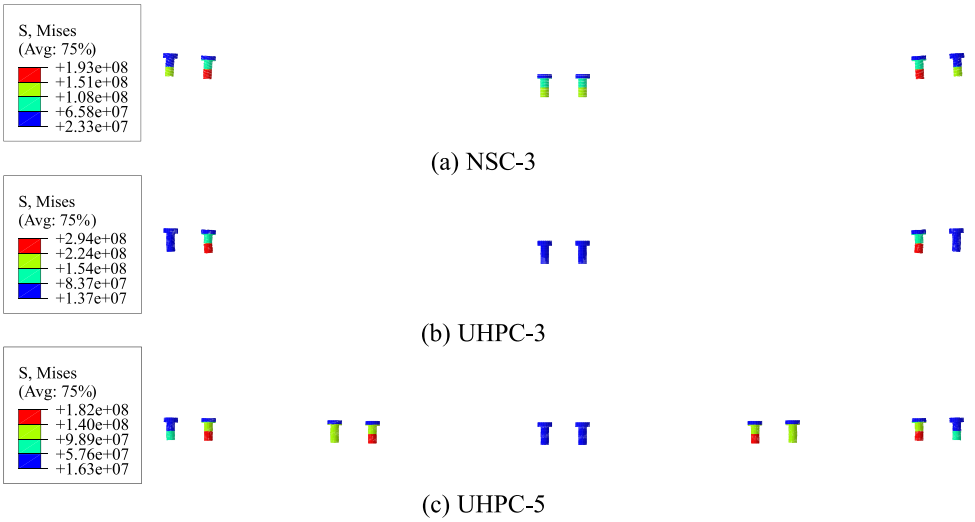

Fig. 12. Von-Mises stress contour of the bolts.

d_u are their corresponding deflections, and u_d is the ductility. The suffix "E" and "S" represent experimental and simulated results, respectively.

From the Fig. 13 and Table 2, it can be seen that the simulated results are in good accordance with the experimental results. The bearing capacity of specimen UHPC-3 with precast UHPC slab is 7.4% greater than that of specimen NSC-3 with precast concrete slab, and the ultimate deflection and ductility improve by 49.2% and 6.6%, respectively. The composite beam with precast UHPC slab with good toughness exhibits good deformation ability.

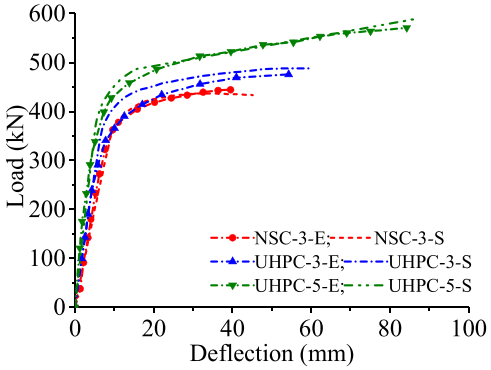

Fig. 13. Comparison of experimental and simulated load-deflection curves.

Table 2
Comparison between the experimental and simulated yield and ultimate loads, corresponding deflections and ductility.

No.	P_y (kN)			d_y (mm)			P_u (kN)			d_u (mm)			u_d		
	$P_{y,E}$	$P_{y,S}$	$P_{y,S}/P_{y,E}$	$d_{y,E}$	$d_{y,S}$	$d_{y,S}/d_{y,E}$	$P_{u,E}$	$P_{u,S}$	$P_{u,S}/P_{u,E}$	$d_{u,E}$	$d_{u,S}$	$d_{u,S}/d_{u,E}$	$u_{d,E}$	$u_{d,S}$	$u_{d,S}/u_{d,E}$
NSC-3	390.4	397.4	1.02	13.3	13.0	0.97	442.7	436.0	0.98	36.4	36.9	1.01	390.4	397.4	1.02
UHPC-3	416.1	435.4	1.05	17.6	16.7	0.95	475.4	487.9	1.03	54.3	54.9	1.01	416.1	435.4	1.05
UHPC-5	497.0	497.8	1.00	25.3	24.1	0.95	570.7	578.6	1.01	84.3	84.5	1.00	497.0	497.8	1.00
Avg			1.02			0.96			1.01			1.01			1.02
Cov			0.02			0.01			0.02			0.01			0.02

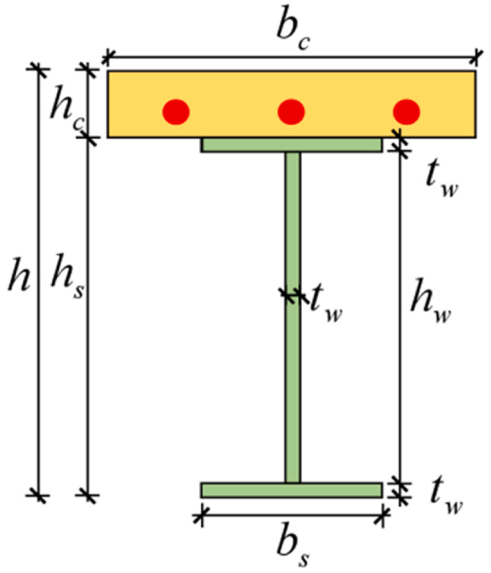

Fig. 14. Cross-section of the section steel-UHPC composite beam.

The bearing capacity of specimen UHPC-5 with more post-pouring belts (that is the shear bolts) is 20.0% greater than that of specimen UHPC-3 with less post-pouring belts, and the ultimate deflection and ductility enhance by 55.2% and 19.4%, respectively. The number of bolts of specimen UHPC-5 is greater than that of specimen UHPC-3, the shear connectors can sustain a higher shear force and enhance the cooperative working performance of composite beam. Thus, the bearing capacity is improved accordingly.

The average value of $P_{y,S}/P_{y,E}$, $d_{y,S}/d_{y,E}$, $P_{u,S}/P_{u,E}$, $d_{u,S}/d_{u,E}$ and $u_{d,S}/u_{d,E}$ are 1.02, 0.96, 1.01, 1.01 and 1.02, respectively, while their coefficient of variation are 0.02, 0.01, 0.02, 0.01 and 0.02, respectively, illustrating that the simulated results fit well with the experimental results.

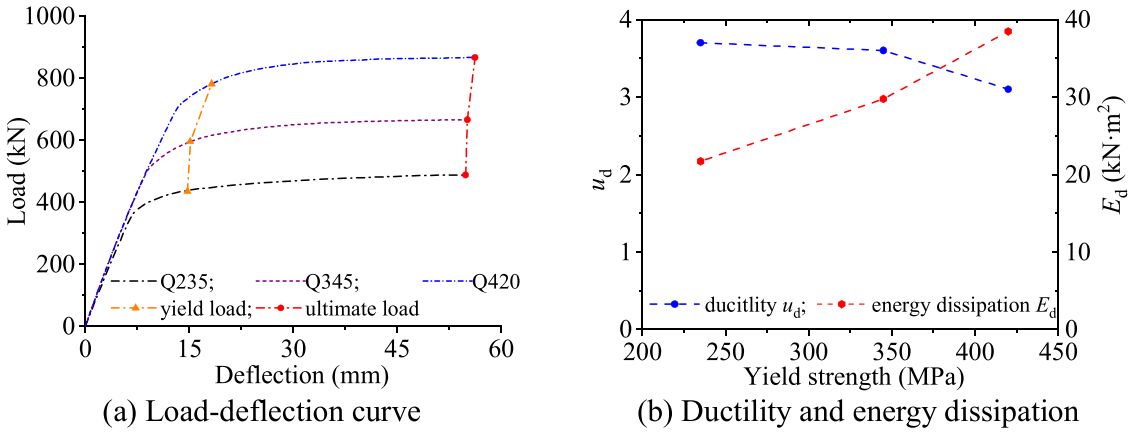

Fig. 15. The effect of strength of section steel.

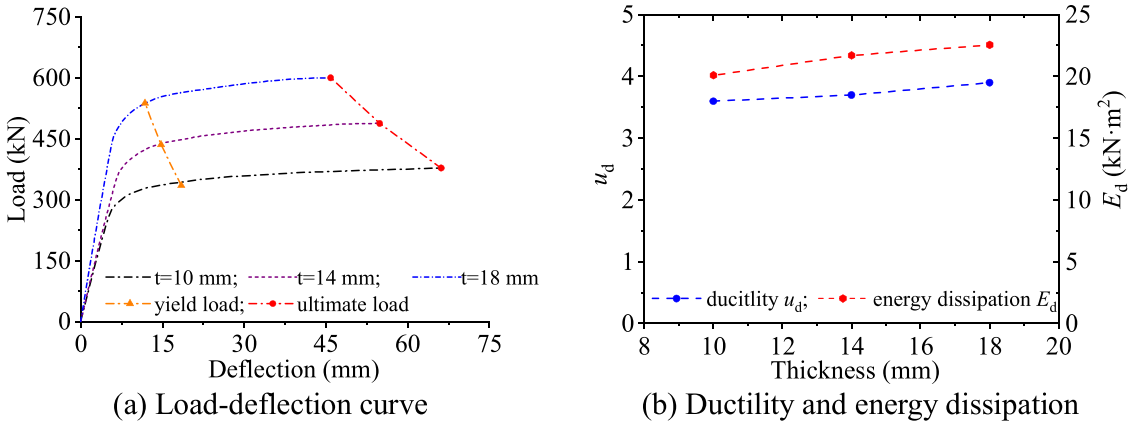

Fig. 16. The effect of thickness of section steel.

4. Parametric studies

In this section, 21 additional FE models are established to study the effects of strength of section steel (that is the yield strength), thickness of section steel (the thickness of flange t_f is assumed the same as that of web t_w, that is $t_f = t_w$), performance of the concrete, height of concrete slab h_c, width of concrete slab b_c, reinforcement of precast slab (that is the diameter of reinforced steel bars) and the diameter of shear bolt, on flexural performance of section steel-UHPC composite beam. Fig. 14 shows the cross-section of the steel-UHPC composite beam, h_w, h_s and h are the height of web of steel beam, section steel and composite beam, respectively, b_s is the width of section steel. The basic parameters, including the dimensions, mechanical properties of the constituent materials, and boundary conditions, are the same as those of specimen UHPC-3 tested.

4.1. Strength of section steel

The effect of strength of section steel on flexural behavior of composite beam is shown in Fig. 15, the yield strength of Q235, Q345 and Q420 steel are 235.0, 345.0 and 420.0 MPa, respectively.

As can be seen from the figure, compared with specimen made of Q235 steel, the yield and ultimate loads of specimen made of Q345 steel improve by 36.8% and 36.5%, respectively, and corresponding deflections improve by 2.9% and 0.5%, respectively. The yield and ultimate load of specimen made of Q420 steel improve by 79.6% and 77.6%, respectively, and corresponding deflection improve by 23.8% and 2.5%, respectively. With the increase of strength of section steel, the yield and ultimate loads of composite beam significantly improve, but the ultimate deflection almost keeps constant. The ductility of specimen made of Q345 and Q420 steel decrease by 2.7% and 16.2%, respectively, but the energy dissipation improve by 37.1% and 77.2%, respectively. Under the same load applied, before the yielding of steel, the strains in the bottom flange of section steels are the same as each other. Thus, the load-deflection curves are almost the same before the yielding. With increasing the strength of section steel, the yield strain and yield strength of the section steel also increase. The yield load and corresponding deflection of specimen with high strength steel are greater than those of specimen with low strength steel. As the yield displacement of the composite beam increases gradually, the ultimate

Table 3
Mechanical properties of concrete analyzed.

No.	E_c (GPa)	ν	f_{cu} (MPa)	f_c (MPa)	f_t (MPa)	ε_{co} (10^{-6})	ε_{cu} (10^{-6})	ε_{tu} (10^{-6})
C40	33.8	0.20	44.7	29.9	2.8	1640	3772	114
C80	38.3	0.20	85.6	53.7	3.5	1964	3633	128
UHPC	42.9	0.21	141.4	124.4	11.1	3281	4921	254

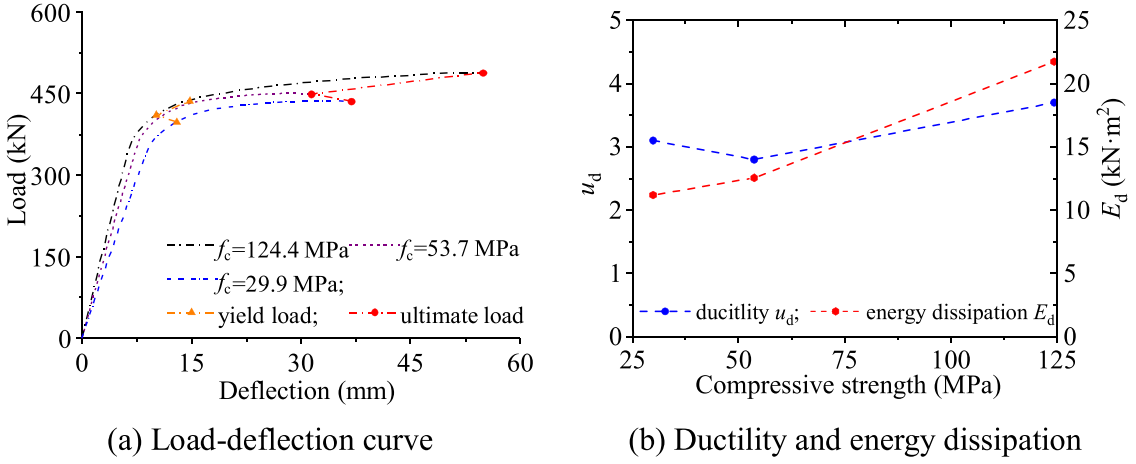

Fig. 17. The effect of concrete performance.

displacement changes little, resulting in a gradual decrease in ductility. After the yielding of steel, the strain of specimen with high strength steel is less than that of specimen with low strength steel, results in a smaller deformation accordingly. The improvement of strength of section steel results in a decrease of ductility, but a significant increase of energy dissipation.

4.2. Thickness of section steel

The effect of thickness of section steel on flexural behavior of composite beam is shown in Fig. 16, the thickness of section steel are 10.0, 14.0 and 18.0 mm, respectively.

As can be seen from the figure, compared with the specimen made of thickness of 10 mm section steel, the yield and ultimate loads of specimen made of thickness of 14 mm section steel improve by 29.9% and 29.0%, respectively, and their corresponding deflections decrease by 20.3% and 17.0%, respectively. The yield and ultimate load of specimen made of thickness of 18 mm section steel improve by 60.5% and 58.8%, respectively, and their corresponding deflection reduce by 36.1% and 30.6%, respectively. As the section steel thickness increases, the tensile strain at its bottom gradually decreases, resulting in a decrease in the composite beam's yield displacement. Besides, the resultant force of the tensile zone also increases, and as a result, the ultimate bearing capacity of the composite beam also increases. In response to the crushing of the concrete slab, the tensile strain at the bottom decreases. This results in a gradual decrease in the ultimate displacement of the composite beam. The ductility of specimen made of thickness of 14 mm and 18 mm steel improve by 2.8% and 8.3%, respectively, but the energy dissipation improve by 8.0% and 12.3%, respectively. With the increase of thickness of section steel, the yield and ultimate loads as well as the ductility and energy dissipation increase, but the yield and ultimate deflections decrease.

4.3. Mechanical properties of concrete

The mechanical properties of concrete compared are listed in Table 3, where E_c is the modulus of elastic, ν is the Poisson's ratio, f_{cu} is the cubic compressive strength, f_c is the compressive strength, f_t is the tensile strength (peak stress) and ε_{tu} is the corresponding strain, ε_{co} and ε_{cu} are the strains corresponding to peak compressive stress and ultimate compressive strength.

The effect of concrete performance on flexural behavior of composite beam is shown in Fig. 17.

It can be seen from the figure, compared with the specimen made of concrete C40, the yield and ultimate loads of specimen made of concrete C80 improve by 3.3% and 3.0%, respectively, and their corresponding deflections reduce by 21.5% and 15.0%, respectively. The yield and ultimate load of specimen made of UHPC improve by 9.6% and 11.9%, respectively, and their corresponding deflection improve by 13.7% and 48.7%, respectively. At failure state, the tensile strain of the bottom steel of the specimen with UHPC is greater than that of the specimen with C40 or C80 leading to greater ultimate section curvature and deformation. Besides, the yield and ultimate loads of composite beam gradually increase with the increase of strength of concrete. As the ultimate compressive strain of concrete C40 is greater than that of concrete C80, but less than that of UHPC, the ultimate deflection of specimen made of UHPC is the

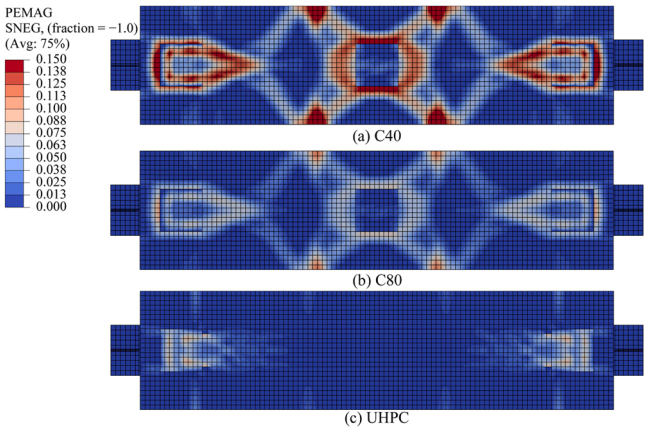

Fig. 18. Cumulative plastic strain (unit: mm/mm).

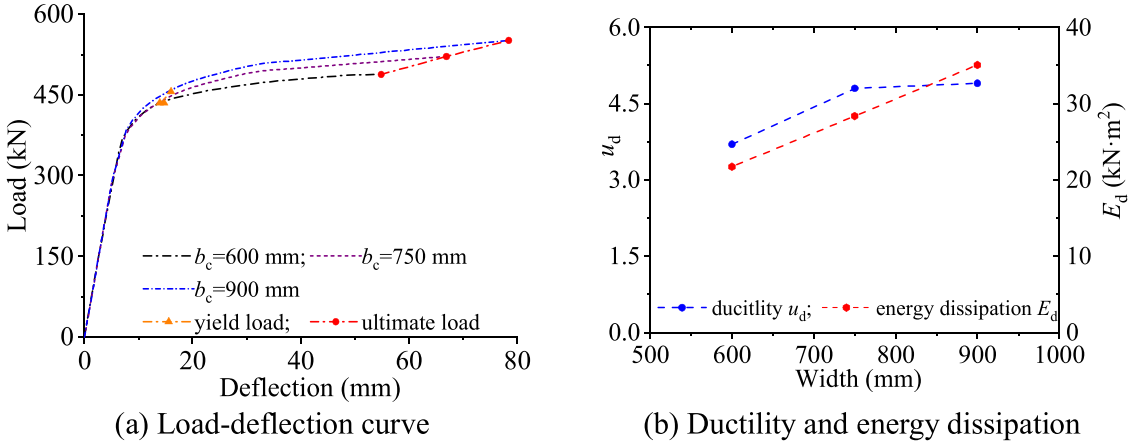

Fig. 19. The effect of width of precast slab.

largest, that of specimen made of concrete C80 is the smallest, and that of specimen made of concrete C40 is in-between. Thus, the ductility of specimen made of UHPC is the highest, that of specimen made of concrete C80 is the lowest, and that of specimen made of concrete C40 is in-between. Compared with specimen made of concrete C40, the energy dissipation of concrete C80 and UHPC improve 12.1% and 94.1%, respectively. The energy dissipation increases with the increase of concrete strength.

Fig. 18 shows the contour plots of cumulative plastic strain (PEMAG). The cumulative plastic strain is a scalar quantity that expresses the inelastic deformation of a material. The larger the value, the higher the degree of plasticity and the greater degree of cumulative damage. With the increase of NSC strength, the cumulative damage decreases gradually. The value of UHPC is the smallest, which indicates that steel-UHPC composite beam has a good bending resistance. In summary, UHPC reduces the development of cracks and improves the durability of the composite beam effectively. It is recommended to use UHPC as a compressive material for the upper part of the composite beam in design and construction to achieve a higher safety factor.

4.4. Size of precast slab

4.4.1. Width of precast slab

The effect of width of precast slab on flexural behavior of composite beam is shown in Fig. 19, the widths are 600, 750 and 900 mm, respectively.

As can be seen from the figure, compared with the specimen having concrete slab with width of 600 mm, the yield load and corresponding deflection almost keep constant. The ultimate load of specimen having concrete slab with width of 750 and 900 mm improve by 6.9% and 13.0%, respectively, and their corresponding deflections improve by 22.0% and 43.0%, respectively. With the increase of the width of concrete slab, the ultimate load and deflection gradually increase. The ductility improve by 29.7% and 32.4%, respectively, and the energy dissipation improve by 30.5% and 61.4%, respectively. The concrete slab with wider width can sustains greater compression than that with smaller width, results in a greater tensile strain at the bottom flange of section steel. The internal force arm (distance between the resultant points of compression and tension force) of specimen with wider concrete slab is greater than

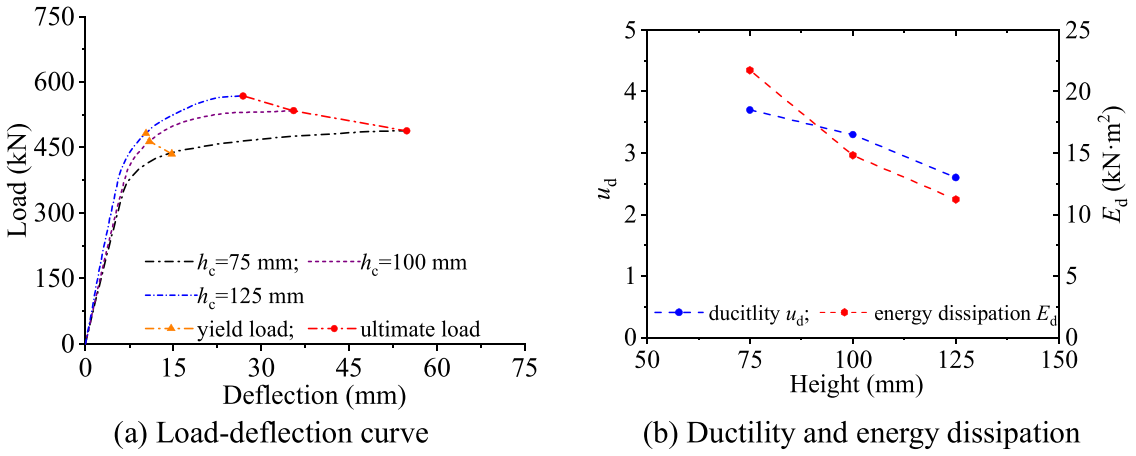

Fig. 20. The effect of height of precast slab.

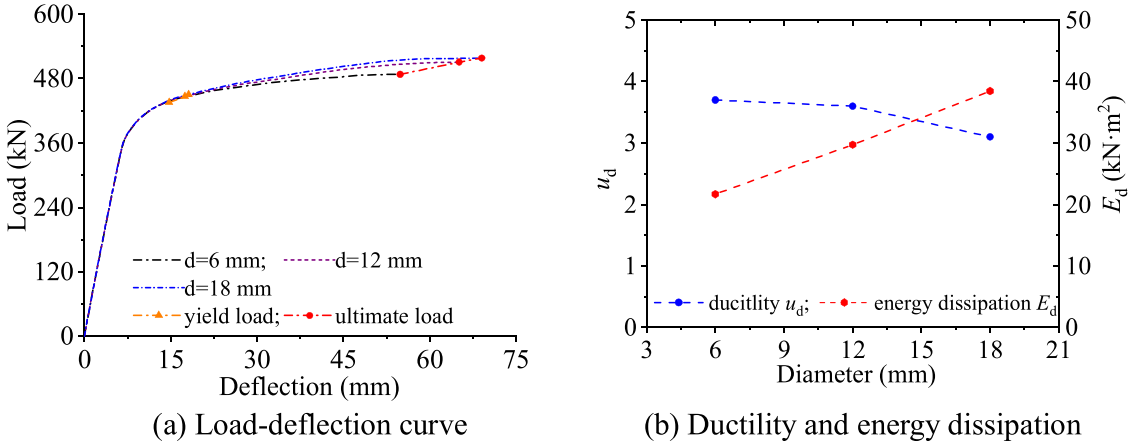

Fig. 21. The effect of reinforcement ratio precast slab.

that of specimen with smaller concrete slab. Thus, with the increase of width of concrete slab, the bearing capacity, ultimate deflection, ductility and energy dissipation of composite beam gradually increase.

4.4.2. Height of precast slab

The effect of height of precast slab on flexural behavior of composite beam is shown in Fig. 20, the heights are 75, 100 and 125 mm, respectively.

As can be seen from the figure, compared with the specimen having concrete slab with height of 75 mm, the yield load and ultimate loads of specimen having concrete slab with height of 100 mm improve by 6.4% and 9.5%, respectively, their corresponding deflections decrease by 25.9% and 35.2%, respectively. The yield load and ultimate loads of specimen having concrete slab with height of 125 mm improve by 10.8% and 16.4%, respectively, their corresponding deflections decrease by 30.0% and 50.9%, respectively. With the increase of height of concrete slab, the yield and ultimate load of composite beam gradually increase, their corresponding deflections gradually decrease. Besides, the moment resistance generated by concrete pressure and steel tension increases (the value and arm of force increase simultaneously) and therefore, the ultimate bearing capacity increases. The ductility of specimen having concrete slab with height of 100 and 125 mm decrease by 10.8% and 29.7%, respectively, and the energy dissipation decrease by 31.9% and 48.4%, respectively. The concrete slab with larger height can sustains greater compression than that with smaller height, results in an improvement of bearing capacity. With the increase of the height of concrete slab, the moment of inertia of composite specimen gradually increases, results in a decrease of deflection. Thus, the ductility and energy dissipation of composite beam gradually decrease. It should be noted that the impact of changing concrete height and width on composite beams varies when compare Fig. 20 (a, b) with Fig. 19 (a, b). There is evidence that the height of concrete has a significant effect on improving the bearing capacity of composite beams, but the effect gradually decreases as the height of concrete increases. Deformation ability of composite beams is affected more by the width of concrete, but this effect decreases with the increase of width.

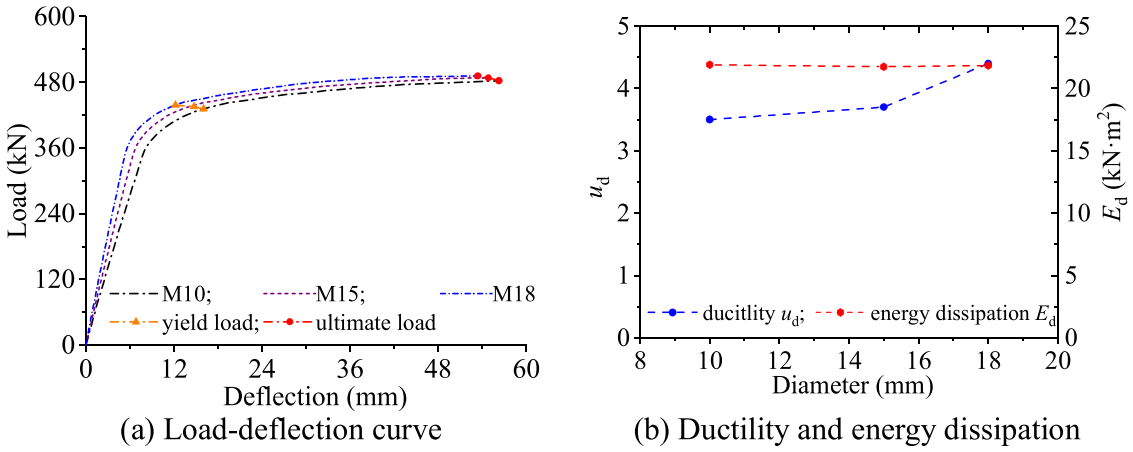

Fig. 22. The effect of diameter of bolt.

4.5. Reinforcement ratio of concrete slab

The effect of diameter of steel bar (that is the reinforcement ratio) reinforced in precast slab on flexural behavior of composite beam is shown in Fig. 21, the diameters are 6, 12 and 18 mm, respectively.

As can be seen from the figure, compared with the specimen with concrete slab reinforced with steel bars having diameter of 6 mm, the yield load and ultimate loads of specimen with concrete slab reinforced with steel bars having diameter of 12 mm only improve by 2.6% and 4.7%, respectively, but their corresponding deflections increase by 18.5% and 18.7%, respectively. The yield load and ultimate loads of specimen with concrete slab reinforced with steel bars having diameter of 18 mm only improve by 3.4% and 6.2%, respectively, but their corresponding deflections increase by 22.9% and 25.8%, respectively. With the increase of reinforcement ratio of concrete slab, the yield and ultimate loads of composite beam slightly increase, but their corresponding deflections significantly increase. Due to the fact that the upper compression is mainly provided by UHPC, the change in reinforcement ratio has little effect on the compressive capacity of the upper compression area, resulting in a relatively small change in the ultimate load. The ductility of specimen with concrete slab reinforced with steel bars having diameter of 12 and 18 mm decrease by 2.7% and 16.2%, respectively, but the energy dissipation increase by 37.1% and 77.2%, respectively.

4.6. Diameter of shear bolt

The effect of diameter of shear bolt on flexural behavior of composite beam is shown in Fig. 22, the diameters are 10, 15 and 18 mm, respectively.

As can be seen from the figure, the effect of diameter of shear bolt on yield and ultimate loads, ultimate defection and energy dissipation of composite beam is slight. Compared with the specimen having shear bolts with diameter of 10 mm, the yield deflection of specimen having shear bolts with diameter of 18 mm decreases by 23.9%, and its ductility increases by 25.7%. With the increase of diameter of shear bolt, the failure mode changes from the rupture of shear bolt to concrete crushing after the yielding of section steel. The shear capacity of the interface between concrete and section steel increases with increasing the bolt diameter. Furthermore, the slip between the interfaces is gradually reduced, and concrete and steel work better together. In general, a suitable increase in bolt diameter can improve the bending stiffness of composite beams before yielding and increase the ultimate load of the composite beam.

5. Bearing capacity of steel-UHPC composite beam

In order to achieve a simplified calculate method for bearing capacity of section steel-UHPC composite beam occurred bending failure, the following assumptions have been taken into account. 1) No slip occurs between the section steel and UHPC. 2) The strain on the cross-section consistent with the plane-section assumption. 3) The specimens considered to be failed either the extreme tensile steel or UHPC compressive fiber reaches their respective ultimate strain. 4) The compression steel bars reinforced in the UHPC slab is neglected.

5.1. Failure mode and discrimination method

For section steel-UHPC composite beam occurs bending failure, there exists three types of failure modes as shown in Fig. 23 and their details are listed as following. The symbols for the dimension of cross-section has been explained in the Section 4, ε_{cu}, ε_{sy} and ε_{su} are the UHPC ultimate compressive strain, the yield and ultimate strain of section steel, respectively; ε_c and ε_s are the maximum UHPC compressive strain (the fiber at the top) and tensile strain of section steel (the fiber at the bottom), respectively.

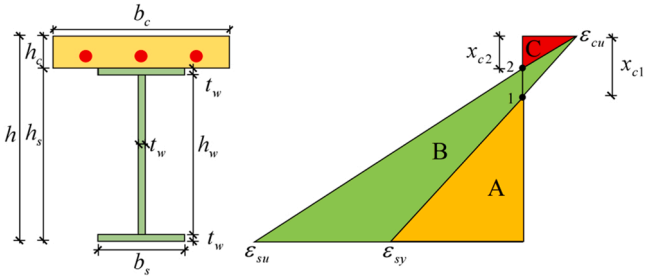

Fig. 23. Failure modes and boundary failure states.

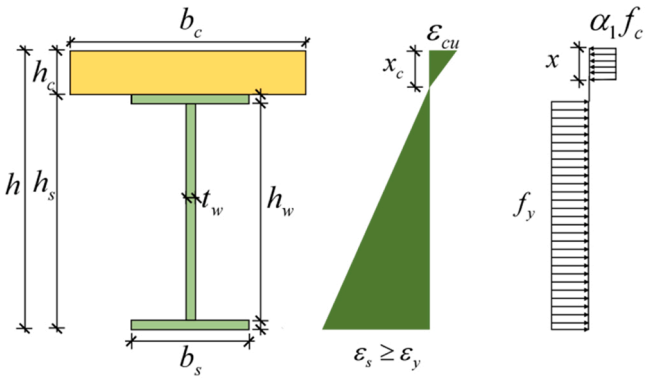

Fig. 24. Cross-section strain and simplified stress distributions-section type I.

(1) Failure mode A: $\varepsilon_c = \varepsilon_{cu}$, $\varepsilon_s < \varepsilon_{sy}$. The compression UHPC reaches its ultimate compressive strain, but the maximum tensile strain of section steel has not yield. This failure mode is similar to the failure mode of over-reinforced RC beams, and is not recommended in engineering structures for its brittleness.
(2) Failure mode B: $\varepsilon_c = \varepsilon_{cu}$, $\varepsilon_{sy} < \varepsilon_s \leq \varepsilon_{su}$. The compression UHPC reaches its ultimate compressive strain after the yielding of section steel, and the maximum tensile strain of section steel is less than its ultimate strain. This failure mode is similar to the failure mode of proper-reinforced RC beams, and is recommended in engineering structures for its ductility and efficient utilization of materials strengths.
(3) Failure mode C: $\varepsilon_c < \varepsilon_{cu}$, $\varepsilon_s = \varepsilon_{su}$. The maximum tensile strain of section steel reaches its ultimate strain while the compression UHPC not, namely, the section steel ruptures before the crushing of UHPC. This failure mode is similar to the failure mode of under-reinforced RC beams, and is not recommended in engineering structures for its brittleness.

Among the three types of failure modes, there exists two boundary failures states as shown in Fig. 23, x_{c1} and x_{c2} are the height of compression zone at boundary failure states 1 and 2, respectively.

(1) Boundary failure 1: $\varepsilon_c = \varepsilon_{cu}$, $\varepsilon_s = \varepsilon_{sy}$. The compression UHPC reaches its ultimate compressive strain and the maximum tensile strain of section steel yields at the same time. That is the crushing of UHPC and yielding of section steel occur simultaneously. Here, the height of compression zone $x_{c1} = \varepsilon_{cu}/(\varepsilon_{cu} + \varepsilon_{sy})h$.
(2) Boundary failure 2: $\varepsilon_c = \varepsilon_{cu}$, $\varepsilon_s = \varepsilon_{su}$. The compression UHPC and the maximum tensile strain of section steel reach their respectively ultimate strain at the same time. That is the crushing of UHPC and rupture of section steel occur simultaneously. Here, the height of compression zone $x_{c2} = \varepsilon_{cu}/(\varepsilon_{cu} + \varepsilon_{su})h$.

So, if the height of compression zone $x_c > x_{c1}$, failure mode A occurs; if $x_{c2} \leq x_c \leq x_{c1}$, failure mode B occurs; if $x_c < x_{c2}$, failure mode C occurs.

5.2. Calculate formulae for bearing capacity

5.2.1. Section type I ($x_c \leq h_c$)

If the height of compression zone x_c smaller than the height of UHPC slab h_c, that is the neutral axial is in the UHPC slab, specimen occurs section type I failure mode. The cross-section strain and simplified stress distributions are shown in Fig. 24.

The following formula can be obtained according to the force equilibrium of cross-section, where x is the calculate height of compressive UHPC, $x = \beta_c x_c$, a_c and β_c are coefficients related to the mechanical properties of UHPC [25]. And it is assumed that the

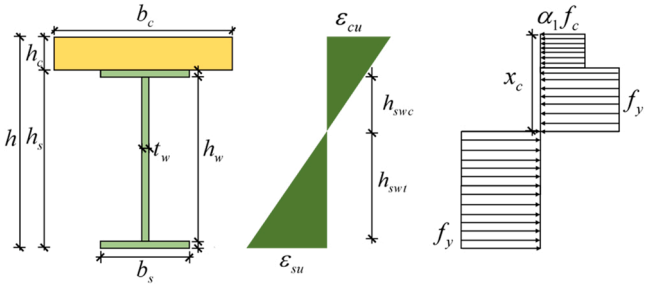

Fig. 25. Cross-section strain and simplified stress distributions-section type II.

lower flange and web of section steel are all yielded, and the tension of upper flange is neglected.

$$\alpha_c f_c b x = f_y\left[\left(b_s - t_w\right)t_w + \left(h_s - t_w\right)t_w\right] \tag{2}$$

Solving for x, Eq. (3) can be obtained.

$$x = \alpha_c \frac{f_y}{f_c}\frac{t_w}{b}\left(b_s + h_s - 2t_w\right) \tag{3}$$

As the height of compression zone should smaller than the height of UHPC slab ($x_c \le h_c$) and $x = \beta_c x_c$, so, the obtained x should less than $\beta_c h_c$, that is $x \le \beta_c h_c$. Taking the resultant point of UHPC compression zone as inertia axis, the moment capacity M_u can be obtained as below.

$$M_u = f_y\left(b_s + h_s - 2t_w\right)t_w\left(h_c + h_s/2 - x/2\right) \tag{4}$$

5.2.2. Section type II ($x_c > h_c$)

If the height of compression zone x_c greater than the height of UHPC slab h_c, that is the neutral axial is in the section steel, specimen occurs section type II failure mode. The cross-section strain and simplified stress distributions are shown in Fig. 25.

The following formula can be obtained according to the force equilibrium of cross-section. And it is assumed that the upper flange under compression and bottom flange under tension, web of section steel under compression and tension are all yielded.

$$\alpha_c f_c b h_c + f_y\left[b_s t_w + \left(x_c - h_c - t_w\right)t_w\right] = f_y\left[b_s t_w + \left(h_s + h_c - x_c - t_w\right)t_w\right] \tag{5}$$

Solving for x, Eq. (6) can be obtained.

$$x_c = h_s \Big/ 2 + h_c - \frac{\alpha_c f_c b h_c}{2 f_y t_w} \tag{6}$$

The height of web of section steel under tension h_{wt} can be obtained as following.

$$h_{swt} = h_s + h_c - x_c - t_w \tag{7}$$

The height of web of section steel under compression h_{wc} can be obtained as following.

$$h_{swc} = x_c - h_c - t_w \tag{8}$$

The distance between the resultant point of compression zone and the upper edge of UHPC slab can be obtained as following.

$$d_c = \frac{\alpha_c f_c b h_c^2/2 + f_y t_w\left[b_s\left(h_c + t_w/2\right) + h_{swc}\left(h_c + t_w + h_{swc}/2\right)\right]}{\alpha_c f_c b h_c + f_y t_w\left(b_s + h_{swc}\right)} \tag{9}$$

Taking the resultant point of compression zone as inertia axis, the moment capacity M_u can be obtained as below.

$$M_u = f_y b_s t_w\left(h_s + h_c - d_c - t_w/2\right) + f_y h_{swt} t_w\left(h_s + h_c - d_c - t_w - h_{swt}/2\right) \tag{10}$$

5.3. Verification

Comparisons of predicated and simulated ultimate loads are shown in Table 4, where $P_{u,p}$ and $P_{u,s}$ are the predicated and simulated ultimate loads, respectively, Avg and CoV are the average value and coefficient of variation, respectively. All specimens occur section type I failure mode.

As can be observed from Table 4, the average value and coefficient of variation of $P_{u,p}$ / $P_{u,s}$ are 0.95 and 0.05, respectively, showing good agreement between the predicted and simulated results, indicating the formulae proposed can be used as a reference for engineering design.

Table 4
Comparison of predicted and simulated ultimate loads.

Beam	$P_{u,s}$ (kN)	$P_{u,p}$ (kN)	$P_{u,p}$ / $P_{u,s}$
UHPC	435.4	422.0	0.97
Q345	595.9	555.3	0.93
Q420	781.9	694.7	0.89
t_w= 10 mm	335.1	311.6	0.93
t_w= 18 mm	537.7	524.8	0.98
h_c= 100 mm	534.2	477.9	0.89
h_c= 150 mm	567.9	589.8	1.04
b_c= 750 mm	521.5	508.2	0.97
bc= 900 mm	551.2	517.1	0.94
Avg			0.95
CoV			0.05

6. Conclusions

This study presents the finite element modelling of flexural behaviors of prefabricated section steel-UHPC composite beams with bolt-UHPC shear pocket. The models verified by three prefabricated section steel-concrete/UHPC composite beams are utilized in parametric study to investigate the effects of mechanical performance section steel and concrete, thickness of section steel, diameters of steel bars and shear bolts, width and height of concrete slab, on flexural performance of composite beams. Based on the results analyzed, the following conclusions can be drawn.

1) With the increase of the strength of section steel, the yield and ultimate loads as well as the energy dissipation gradually increase, but the ductility decreases. Compared with composite beam made of Q235 section steel, the ultimate load of beams made of Q345 and Q420 section steel improve by 36.5% and 77.6%, respectively, the energy dissipation improve by 37.1% and 77.2%, respectively, but the ductility decrease by 2.7% and 16.2%, respectively.
2) With the increase of the thickness of section steel, the yield and ultimate loads significantly increase, the ductility and energy dissipation gradually increase. Compared with composite beam made of section steel with thickness of 10 mm, the ultimate load of beams made of section steel with thickness of 14 and 18 mm improve by 29.0% and 58.8%, respectively, the ductility enhance by 2.8% and 8.3%, respectively, and the energy dissipation improve by 8.0% and 12.3%, respectively.
3) With the increase of concrete strength, the ultimate load, deflection and energy dissipation gradually increase. The ductility of steel-UHPC composite beam is the highest, that of steel-HSC composite beam is the lowest. With the increase of the width and height of concrete slab, the ultimate load gradually increases. The ductility and energy dissipation gradually increase with the increase of the width of concrete slab, but decrease with the increase of the height of concrete slab.
4) The effect of reinforcement ratio of concrete slab and diameter of shear bolts on the ultimate load of composite beam is limited. The ultimate deflection increases with the increase of reinforcement ratio of concrete slab, decreases with the increase of diameter of shear bolts. The ductility decreases while the energy dissipation increases, with the increase of the reinforcement ratio of concrete slab. But the ductility increases while the energy dissipation decreases, with the increase of the diameter of shear bolts.
5) Three failure modes and two boundary failure states of section steel-UHPC composite beams are proposed. And simplified formulae for two different types of section proper-reinforced composite beams occurred bending failure developed, the predicted results are in good accordance with simulated results.

Declaration of Competing Interest

The authors declare that they have no known competing financial interests or personal relationships that could have appeared to influence the work reported in this paper.

Data availability

Data will be made available on request.

Acknowledgement

The authors would like to acknowledge the financial support to the work presented in this paper from the High-End Foreign Experts Project of Ministry of Science and Technology, China (G2022014054L), the Natural Science Foundation of Jiangsu Province, China (BK20201436), the Science and Technology Project of Jiangsu Construction System (2018ZD047, 2021ZD06), the Science and Technology Project of Gansu Construction System (JK2021–19), the Opening Foundation of Jiangsu Province Engineering Research Center of Prefabricated Building and Intelligent Construction (2021), the Science and Technology Cooperation Fund Project of Yangzhou City and Yangzhou University (YZ2022194, YZU212105), the Science and Technology Project of Yangzhou Construction System (2022ZD03), the Nantong Jianghai (226) talents project and the Blue Project Youth Academic Leader of Colleges and

Universities in Jiangsu Province (2020).

References

[1] P. Richard, M.H. Cheyrezy, Reactive powder concretes with high ductility and 200–800 MPa compressive strength, Acids Spec. Publ. 144 (1994) 507–518.
[2] W. Wang, X.D. Zhang, X.L. Zhou, B. Zhang, J. Chen, C.H. Li, Experimental study on shear performance of an advanced bolted connection in steel-concrete composite beams, Case Stud. Constr. Mat. 16 (2022), e01037.
[3] S.C. Ma, Y.Y. Lou, P. Bao, Experimental research and numerical analysis of shearing resistance in steel-concrete composite beam connectors, Case Stud. Constr. Mat. 17 (2022), e01210.
[4] Y.J. Zhang, Z.C. Yang, T.Y. Xie, J. Yang, Flexural behaviour and cost effectiveness of layered UHPC-NC composite beams, Eng. Struct. 273 (2022), 115060.
[5] Y. Yu, X.Y. Zhao, J.J. Xu, S.C. Wang, T.Y. Xie, Evaluation of shear capacity of steel fiber reinforced concrete beams without stirrups using artificial intelligence models, Materials 15 (2022) 2407.
[6] S.W. Pathirana, B. Uy, O. Mirza, X.Q. Zhu, Flexural behaviour of composite steel–concrete beams utilising blind bolt shear connectors, Eng. Struct. 114 (2016) 181–194.
[7] Q.W. Yan, Z. Zhang, J. Yan, S. Laflamme, Analysis of flexural capacity of a novel straight-side U-shaped steel-encased concrete composite beam, Eng. Struct. 242 (2021), 112447.
[8] Y.L. Yang, W.T. Liang, Q.J. Yang, Y. Cheng, Flexural behavior of web embedded steel-concrete composite beam, Eng. Struct. 240 (2021), 112345.
[9] S. Gao, Q. Bai, L.H. Guo, S.B. Kang, A. Derlatka, S. Deng, Study on flexural behavior of spliced shallow composite beams with different shear connectors, Eng. Struct. 253 (2022), 113816.
[10] T.J. Lou, S.S. Wu, B. Chen, Effect of reinforcement on the response of continuous steel-concrete composite beams, Case Stud. Constr. Mat. 16 (2022), e00929.
[11] Y. Idris, T. Ozbakkaloglu, Flexural behavior of FRP-HSC-steel composite beams, Thin Wall Struct. 80 (2014) 207–216.
[12] G. Xiong, W. Li, X.D. Wang, J.P. Liu, Y.T. Bai, Y.F. Chen, Flexural behavior of prefabricated high-strength steel-concrete composite beams with steel block connectors, J. Constr. Steel Res 197 (2022), 107507.
[13] J.S. Fan, S.K. Gou, R. Ding, J. Zhang, Z.J. Shi, Experimental and analytical research on the flexural behaviour of steel–ECC composite beams under negative bending moments, Eng. Struct. 210 (2020), 110309.
[14] C.L. Nguyen, C.K. Lee, Flexural behaviours of engineered cementitious composites – high strength steel composite beams, Struct. Eng. 249 (2021), 113324.
[15] Y.Q. Hu, M. Meloni, Z. Cheng, J.Q. Wang, H.L. Xiu, Flexural performance of steel-UHPC composite beams with shear pockets, Structures 27 (2020) 570–582.
[16] Y. Zhang, S.K. Cai, Y.P. Zhu, L. Fan, X.D. Shao, Flexural responses of steel-UHPC composite beams under hogging moment, Eng. Struct. 206 (2020), 110134.
[17] J.S. Zhu, X.Y. Guo, J.F. Kang, M.H. Duan, Y.G. Wang, Numerical and theoretical research on flexural behavior of steel-UHPC composite beam with waffle-slab system, J. Constr. Steel Res 171 (2020), 106141.
[18] J.P. Liu, Z.C. Lai, B.C. Chen, S. Xu, Experimental behavior and analysis of steel-laminated concrete (RC and UHPC) composite girders, Eng. Struct. 225 (2020), 111240.
[19] Z.C. Fang, H.Z. Fang, P.J. Li, H.B. Jiang, G.F. Chen, Interfacial shear and flexural performances of steel–precast UHPC composite beams: Full-depth slabs with studs vs. demountable slabs with bolts, Eng. Struct. 260 (2022), 114230.
[20] L.W. Tong, L.H. Chen, X.Q. Wang, J. Zhu, X.D. Shao, Z. Zhao, Experiment and finite element analysis of bending behavior of high strength steel-UHPC composite beams, Eng. Struct. 266 (2022), 114594.
[21] Y.J. Zhang, J.P. Zhang, A.R. Liu, B.C. Chen, B. Safaei, Z.C. Yang, Study on the behavior of high-strength friction-grip bolts under combined shear and tensile forces, Struct 45 (2022) 854–866.
[22] X.D. Shao, X.D. Zhao, Q. Liu, S.W. Deng, Y. Wang, Design and experimental study of hot rolled shape steel-ultrahigh performance concrete composite beam, Eng. Struct. 252 (2022), 113612.
[23] H.L. Wang, T. Sun, C. Tang, Experimental and numerical investigation of steel ultra-high-performance concrete continuous composite beam behavior, Eng. Struct. 23 (2020) 2220–2236.
[24] R.S. Nicoletti, A. Rossi, A.S.C. Souza, C.H. Martins, Numerical assessment of effective width in steel-concrete composite box girder bridges with partial interaction, Eng. Struct. 239 (2021), 112333.
[25] GB 50010-2010, Code for design of concrete structures, Beijing (2010).
[26] B. Shan, Experiment and research on basic mechanical properties of reactive powder concrete, Hu'nan University, Changsha, 2002 (in Chinese).
[27] E. Baran, M. Mahamid, M. Baran, M. Kurtoglu, I. Torra-Bilal, Performance of a moment resisting beam-column connection for precast concrete construction, Eng. Struct. 246 (2021), 113005.
[28] M. Singh, A.H. Sheikh, A.M.S. Mohamed, P. Visintin, M.C. Griffith, Experimental and numerical study of the flexural behaviour of ultra-high performance fibre reinforced concrete beams, Constr. Build. Mater. 138 (2017) 12–25.
[29] I. Arrayago, E. Real, L. Gardner, Description of stress-strain curves for stainless steel alloys, Mater. Des. 87 (2015) 540–552.
[30] Z.H. Guo, X.D. Shi, Reinforce concrete theory and analyse, Beijing: Tsinghua university press, 2003, pp. 163–337.